

Light clusters as a possible source of crustal impurities: a quasi-particle approach

Helena Pais^{1*}, Hoa Dinh-Thi², Anthea F. Fantina³, Francesca Gulminelli⁴, and Constança Providência¹

¹CFisUC, University of Coimbra, P-3004-516 Coimbra, Portugal.

²Department of Physics and Astronomy - MS 108, Rice University, 6100 Main Street, Houston, TX 77251-1892, USA.

³Grand Accélérateur National d'Ions Lourds (GANIL), CEA/DRF - CNRS/IN2P3, Boulevard Henri Becquerel, 14076 Caen, France.

⁴Université Normandie, ENSICAEN, LPC-Caen, 14000 Caen, France.

Received xxx Accepted xxx

ABSTRACT

Context. The presence of impurities in the neutron star crust is known to affect in an important way the thermal and electrical conductivity of the star.

Aims. In this work, we explore the possibility that such impurities might arise from the simultaneous presence of heavy ions together with Hydrogen and Helium isotopes formed during the cooling process of the star.

Methods. We consider an equilibrium population of such light particles at temperatures close to the crystallization of the crust within an effective quasi-particle approach including in-medium binding energy shifts, and using different versions of the relativistic mean field approach for the crustal modeling. Thermal effects are consistently included also in the dominant ion species present in each crustal layer described in the compressible liquid drop approximation.

Results. We find that the impurity factor associated to light clusters is comparatively very small and can be neglected in transport calculations, even if a strong model dependence is observed.

Key words. stars: neutron – equation of state – dense matter

1. Introduction

Light nuclear clusters such as Hydrogen or Helium isotopes are expected to be produced in hot and dense stellar matter, and their abundance is known to affect the dynamical properties of core-collapse supernovae (Arcones et al. 2008; Sumiyoshi & Roepke 2008; Furusawa et al. 2013, 2017; Fischer et al. 2014, 2020) and binary neutron star (NS) mergers (Bauswein et al. 2013; Rosswog 2015; Radice et al. 2018; Psaltis et al. 2024). Even if the weak rates directly involving light clusters are low (Fischer et al. 2020), their abundance is in competition with the one of heavy nuclei (Pais et al. 2019), which indirectly affects the neutrino dynamics, and the size and proton fraction of the nucleosynthesis seeds (Nedora et al. 2021).

The possible relevance of light clusters in NS physics is much less addressed in the literature. In this paper, we explore the possibility that such light composites might play the role of impurities in the crustal lattice. Formed from core-collapse supernova explosions, NSs are indeed born hot, with temperatures exceeding several MeV (Haensel et al. 2007). In these conditions, the crust of the proto-NS is a liquid plasma composed of different nuclear species including light clusters in a background of electrons and nucleons. It is generally assumed that, as the NS crust cools down, this multi-component plasma remains in full thermodynamic equilibrium until the crust crystallizes, and that the composition at the crystallization temperature coincides with the ground-state composition, namely a se-

quence of pure layers, each consisting of a one-component ideal Coulomb crystal. In this situation, the only nuclear species relevant for the description of a NS are heavy ions with atomic numbers of the order $Z \approx 20 - 40$.

However, the crustal lattice is not expected to be strictly perfect, and can present different defects that are collectively known as impurities and quantified via an “impurity parameter” that measures the importance of charge fluctuations at each depth of the crust. In the magnetothermal simulations of NS evolution, this (possibly density-dependent) impurity parameter is typically adjusted on observational cooling data (Viganò et al. 2013). A high value for the impurity parameter lowers the electrical and thermal conductivity, and seems to be needed for a better description of different astrophysical observations concerning isolated X-ray pulsars and late time cooling in binaries (Pons et al. 2013; Newton 2013; Deibel et al. 2017; Hambaryan et al. 2017; Tan et al. 2018).

If the presence of highly resistive layers due to the presence of impurities seems well settled, its physical origin and the actual value of the impurity parameter are less clear. Classical molecular dynamics simulations suggest that the innermost part of the inner crust is composed of disordered and amorphous nuclear matter, with coexistence of different exotic complex shapes (Schneider et al. 2014; Horowitz et al. 2015; Caplan et al. 2021; Newton et al. 2022). The onset of this pasta mantle is, however, model dependent (Dinh Thi, H. et al. 2021; Shchekilin et al. 2023) and the most extended part of the inner crust is believed to be composed of stan-

* hpais@uc.pt

dard spherical nuclei (Shchekilin et al. 2024). In the spherical regime, if the one-component plasma approximation is released, it was suggested that different ion species might persist as impurities in the whole catalyzed crust, due to the non-adiabaticity of the cooling dynamics (Goriely et al. 2011; Fantina et al. 2020; Carreau et al. 2020; Potekhin & Chabrier 2021; Dinh Thi et al. 2023b). In particular, the authors of Refs. Fantina et al. (2020); Dinh Thi et al. (2023b) computed the impurity factor self-consistently within a multi-component approach at different temperatures close to the crystallization temperature. They found that high values of the impurity parameter between $Q_{\text{imp}} \approx 5$ and $Q_{\text{imp}} \approx 100$ can be obtained in the inner crust, even in the density region where deformed pasta structures are not expected, due to the simultaneous presence at finite temperature of light ($Z \approx 2 - 3$) and heavy ($Z \approx 20 - 30$) ions. In that study, a single energy functional was employed, and the cluster free energy was computed with the compressible liquid drop (CLD) model, which gives a poor description of the lightest nuclei. It is therefore interesting to study the model dependence of those results, and to explore a more accurate and microscopic description of the light cluster free energies in a dense nuclear medium.

From the study of Refs. Fantina et al. (2020); Dinh Thi et al. (2023b) we expect that important charge fluctuations can only occur if the charge distribution has a multi-modal structure, with clusters of very different sizes appearing with comparable probability. We therefore consider a simplified theoretical setting where the one-component plasma approximation is kept for the dominant ion species, but Hydrogen and Helium isotopes are additionally added as explicit degrees of freedom, as it was proposed in previous works employing the relativistic mean-field (RMF) approximation for the nuclear interaction (Avancini et al. 2012; Ferreira & Providencia 2012). The advantage of this description is that in-medium modifications of the light cluster energies in the medium are easily introduced as a modification of the couplings of nucleons bound in clusters with the effective mesonic fields (Pais et al. 2018). This effective coupling modification was extensively calibrated on ab-initio calculations (Röpke 2015, 2020; Ren et al. 2024) and experimental constraints (Qin et al. 2012; Bougault et al. 2020) in particular for the FSU functional (Pais et al. 2020; Custódio et al. 2020, 2024). Within this formalism, fluctuations of the dominant ion species in the different Wigner-Seitz cells are neglected, as well as the possible presence of exotic neutron-rich clusters (Pais et al. 2019). The resulting Q_{imp} values will, therefore, represent a lower limit to the crustal impurities.

The paper is organized as follows: in Sect. 2 we introduce the formalism used in this work; specifically, we describe in Sect. 2.1 the treatment of homogeneous matter, in Sect. 2.2 that of the (heavier) clusters through the CLD model, and in Sect. 2.3 the treatment of light clusters. We present our numerical results in Sect. 3, and finally we draw our conclusions in Sect. 4. In this work, we consider natural units, where $\hbar = c = k_B = 1$.

2. Formalism

Each layer of the inner crust of the NS is described as a collection of identical neutral cells constituted of a single spherical nucleus, and a uniform distribution of dripped

neutrons and point-like light clusters, all interacting with and through effective meson fields. The nucleus is treated as a CLD with bulk, surface, and Coulomb terms, in the same spirit as in Ref. Pais et al. (2015). Since we are considering the liquid phase of the crust, translational degrees of freedom are also associated to the nuclear droplet.

In the following subsections we describe in further details the theoretical treatment of homogeneous matter (Sect. 2.1), that is used for the bulk part of the droplet energy as well as for the dripped neutrons, the finite-size and translational terms associated to the nuclear droplet within a CLD model (Sect. 2.2), and the treatment of the light clusters (Sect. 2.3).

2.1. Homogeneous matter

Our formalism is based on the non-linear Walecka model in the mean-field approximation (Furnstahl et al. 1996, 1997), where we consider an infinite homogeneous system of nucleons with mass M (protons p and neutrons n), interacting with and through three meson fields: an isoscalar-scalar field ϕ with mass m_s , an isoscalar-vector field V^μ with mass m_v and an isovector-vector field \mathbf{b}^μ with mass m_ρ , for the isospin dependence. Protons and electrons interact through the electromagnetic field A^μ . The Lagrangian density is given as:

$$\mathcal{L} = \sum_{j=p,n} \mathcal{L}_j + \mathcal{L}_e + \mathcal{L}_\sigma + \mathcal{L}_\omega + \mathcal{L}_\rho + \mathcal{L}_{\omega\rho} + \mathcal{L}_\gamma. \quad (1)$$

The nucleon and electron terms read, respectively,

$$\mathcal{L}_j = \bar{\psi}_j [\gamma_\mu iD^\mu - M^*] \psi_j, \quad (2)$$

$$iD^\mu = i\partial^\mu - g_v V^\mu - \frac{g_\rho}{2} \boldsymbol{\tau} \cdot \mathbf{b}^\mu - e \frac{1 + \tau_3}{2} A^\mu, \quad (3)$$

$$\mathcal{L}_e = \bar{\psi}_e [\gamma_\mu (i\partial^\mu + eA^\mu) - m_e] \psi_e. \quad (4)$$

and the nucleon Dirac effective mass is given as

$$M^* = M - g_s \phi. \quad (5)$$

The meson and electromagnetic fields Lagrangian densities are given by:

$$\begin{aligned} \mathcal{L}_\sigma &= \frac{1}{2} \left(\partial_\mu \phi \partial^\mu \phi - m_s^2 \phi^2 - \frac{1}{3} \kappa \phi^3 - \frac{1}{12} \lambda \phi^4 \right) \\ \mathcal{L}_\omega &= -\frac{1}{4} \Omega_{\mu\nu} \Omega^{\mu\nu} + \frac{1}{2} m_v^2 V_\mu V^\mu + \frac{1}{4!} \xi g_v^4 (V_\mu V^\mu)^2 \\ \mathcal{L}_\rho &= -\frac{1}{4} \mathbf{B}_{\mu\nu} \cdot \mathbf{B}^{\mu\nu} + \frac{1}{2} m_\rho^2 \mathbf{b}_\mu \cdot \mathbf{b}^\mu \\ \mathcal{L}_\gamma &= -\frac{1}{4} F_{\mu\nu} F^{\mu\nu} \\ \mathcal{L}_{\omega\rho} &= \Lambda_v g_v^2 g_\rho^2 \mathbf{b}_\mu \cdot \mathbf{b}^\mu V_\mu V^\mu, \end{aligned}$$

where $\Omega_{\mu\nu} = \partial_\mu V_\nu - \partial_\nu V_\mu$, $\mathbf{B}_{\mu\nu} = \partial_\mu \mathbf{b}_\nu - \partial_\nu \mathbf{b}_\mu - g_\rho (\mathbf{b}_\mu \times \mathbf{b}_\nu)$ and $F_{\mu\nu} = \partial_\mu A_\nu - \partial_\nu A_\mu$. The nonlinear $\mathcal{L}_{\omega\rho}$ term affects the density dependence of the symmetry energy. The models comprise the following parameters: three coupling constants g_s , g_v and g_ρ of the mesons to the nucleons, the mixing $\omega\rho$ coupling, Λ_v , the bare nucleon mass M , the electron mass m_e , the masses of the mesons, the electromagnetic coupling constant $e = \sqrt{4\pi/137}$ and the self-interacting coupling

constants κ , λ , and ξ . In this Lagrangian density, $\boldsymbol{\tau}$ are the Pauli matrices.

Concerning the choice of the nuclear interaction, we use two families of models, non-linear (NL) models, FSU (Todd-Rutel & Piekarewicz 2005), FSU2R (Negreiros et al. 2018), NL3 $\omega\rho$ (Horowitz & Piekarewicz 2001; Pais & Providência 2016), and NLset21 (Malik et al. 2024), whose couplings of the mesons to the nucleons are fixed, and the meson terms included in the Lagrangian density are up to quartic order, as defined above, and density-dependent (DD) models, namely TW (Typel & Wolter 1999), DD2 (Typel et al. 2010) and DDME2 (Lalazissis et al. 2005), whose couplings of the mesons to the nucleons vary with the density. In this case, the self-interaction couplings κ , λ and the mixing $\omega\rho$ coupling Λ_v are zero, and the g_s , g_v and g_ρ couplings are given by the density-dependent functions (Typel & Wolter 1999; Typel et al. 2010; Lalazissis et al. 2005)

$$g_i = g_{i0} f_i(x), \quad i = s, v, \quad (6)$$

$$f_i(x) = a_i \frac{1 + b_i(x + d_i)^2}{1 + c_i(x + d_i)^2}, \quad (7)$$

$$g_\rho = g_{\rho 0} \exp(-a_\rho(x - 1)), \quad (8)$$

with $x = \rho/\rho_0$. The reader can refer to Refs. Typel & Wolter (1999); Typel et al. (2010); Lalazissis et al. (2005) for the values of the parameters a_i, b_i, c_i, d_i for each DD model.

DDME2 was fitted to reproduce the properties of symmetric and asymmetric matter, binding energies and neutron and charge radii of stable nuclei. Moreover, this model is able to reproduce two-solar-mass NSs. DD2 also reproduces finite nuclei properties and is based on the TW model, the first density-dependent model that appeared in the literature. FSU, on the other hand, is not able to produce two-solar-mass NSs, but it describes well the properties of nuclear matter at and below saturation density (Grill et al. 2014), which is the range of densities considered in this work. However, FSU2R was constructed in order to correct the two-solar-mass problem, and differs from FSU in the isovector sector. NLset21 is a recent model chosen from a set of NL models constructed using Bayesian techniques (Malik & Providência 2022) that fulfill astrophysical, chiral effective-field-theory (EFT) neutron-matter calculations, and also reproduce well the symmetric matter properties at saturation. NL3 $\omega\rho$ is a model from the NL3 family, i.e. it has the same isoscalar properties as NL3, but differs in the isovector properties. Since NL3 has a very large slope of the symmetry energy, $L_{\text{sym},0} = 118$ MeV, the NL3 $\omega\rho$ model is constructed by adding a term mixing the ω and ρ mesons in order to lower the value of $L_{\text{sym},0}$: the mixing term is varied and the corresponding isovector coupling is calculated so that the symmetry energy at $\rho = 0.1 \text{ fm}^{-3}$ has the same value as in NL3.

The equilibrium state of asymmetric nuclear matter is characterized by the distribution functions, $f_{0k\pm}$, of particles (+) and antiparticles (-) $k = p, n, e$, given by:

$$f_{0j\pm} = \frac{1}{1 + e^{(\epsilon_{0j} \mp \nu_j)/T}}, \quad j = p, n \quad (9)$$

with

$$\epsilon_{0j} = \sqrt{p^2 + M^{*2}}, \quad \nu_j = \mu_j - g_v V_0^{(0)} - \frac{g_\rho}{2} \tau_j b_0^{(0)} \quad (10)$$

and

$$f_{0e\pm} = \frac{1}{1 + e^{(\epsilon_{0e} \mp \mu_e)/T}}, \quad (11)$$

$$\epsilon_{0e} = \sqrt{p^2 + m_e^2}, \quad (12)$$

where μ_k is the chemical potential of particle $k = p, n, e$. The net particles densities are readily calculated from the distribution functions as

$$\rho_j = \frac{1}{\pi^2} \int dp p^2 (f_{0j+} + f_{0j-}). \quad (13)$$

In the mean-field approximation, the thermodynamic quantities of interest are given in terms of the meson fields, which are replaced by their constant expectation values (denoted by a subscript '0').

For homogeneous neutral nuclear matter, the energy density, the entropy density, the free energy density, and the pressure are given, respectively, by:

$$\begin{aligned} \mathcal{E} &= \frac{1}{\pi^2} \sum_{j=p,n} \int dp p^2 \epsilon_{0j} (f_{0j+} + f_{0j-}) \\ &+ \frac{m_v^2}{2} V_0^2 + \frac{\xi g_v^4}{8} V_0^4 + \frac{m_\rho^2}{2} b_0^2 + \frac{m_s^2}{2} \phi_0^2 \\ &+ \frac{k}{6} \phi_0^3 + \frac{\lambda}{24} \phi_0^4 + 3\Lambda_v g_\rho^2 g_v^2 V_0^2 b_0^2, \end{aligned} \quad (14)$$

$$\begin{aligned} \mathcal{S} &= -\frac{1}{\pi^2} \sum_{j=p,n} \int dp p^2 [f_{0j+} \ln f_{0j+} \\ &+ (1 - f_{0j+}) \ln(1 - f_{0j+}) + f_{0j-} \ln f_{0j-} \\ &+ (1 - f_{0j-}) \ln(1 - f_{0j-})], \end{aligned} \quad (15)$$

$$\mathcal{F} = \mathcal{E} - T\mathcal{S}, \quad (16)$$

$$\begin{aligned} P &= \frac{1}{3\pi^2} \sum_{j=p,n} \int dp \frac{p^4}{\epsilon_{0j}} (f_{0j+} + f_{0j-}) \\ &+ \frac{m_v^2}{2} V_0^2 + \frac{\xi g_v^4}{24} V_0^4 + \frac{m_\rho^2}{2} b_0^2 - \frac{m_s^2}{2} \phi_0^2 \\ &- \frac{k}{6} \phi_0^3 - \frac{\lambda}{24} \phi_0^4 + \Lambda_v g_\rho^2 g_v^2 V_0^2 b_0^2. \end{aligned} \quad (17)$$

For the DD models, there is an extra term in the pressure $P \rightarrow P + \rho \Sigma_0$ with

$$\rho \Sigma_0 = \rho [g'_v V_0 \rho + g'_\rho b_0 (\rho_p - \rho_n) - g'_s \phi_0 \rho_s] \quad (18)$$

with g'_i the derivative of the couplings with respect to the density. This rearrangement term, Σ_0 , appears in the vector self-energy due to the density dependence of the couplings.

For the electrons, we have

$$\mathcal{E}_e = \frac{1}{\pi^2} \int dp p^2 \epsilon_{0e} (f_{0e+} + f_{0e-}), \quad (19)$$

$$\begin{aligned} \mathcal{S}_e &= -\frac{1}{\pi^2} \int dp p^2 [f_{0e+} \ln f_{0e+} + (1 - f_{0e+}) \ln(1 - f_{0e+}) \\ &+ f_{0e-} \ln f_{0e-} + (1 - f_{0e-}) \ln(1 - f_{0e-})], \end{aligned} \quad (20)$$

$$\mathcal{F}_e = \mathcal{E}_e - T\mathcal{S}_e, \quad (21)$$

$$P_e = \frac{1}{3\pi^2} \int dp \frac{p^4}{\epsilon_{0e}} (f_{0e+} + f_{0e-}). \quad (22)$$

2.2. Inhomogeneous matter in the compressible liquid drop model

The simplest treatment of a nucleus immersed in a sea of dripped nucleons is to divide each cell of volume V_W into two separated regions of constant density, such that $V_W = V^I + V^{II}$, the higher density region (I) representing the nucleus, and the lower density one (II) representing the background nucleon gas. The baryonic number and charge of the nucleus are therefore given by:

$$A_{\text{heavy}} = V^I \rho^I, \quad (23)$$

$$Z_{\text{heavy}} = V^I \rho^I y_p^I. \quad (24)$$

In this picture, the interface between the two regions is sharp, and all the thermodynamical quantities are linear combinations of the corresponding quantities in the two phases. In particular, the free energy of a cell reads:

$$\mathcal{F}_W = f\mathcal{F}^I + (1-f)\mathcal{F}^{II} + \mathcal{F}_e, \quad (25)$$

where $f = V^I/V_W$ is the volume fraction of the nucleus, \mathcal{F}_e is given by Eq. (21), and $\mathcal{F}^{I(II)}$ is a short-hand notation for the baryonic free energy density of homogeneous matter (see Eq. (16)) evaluated at densities $(\rho_p^{I(II)}, \rho_n^{I(II)})$.

In the CLD model, the existence of an extended interface between the nucleus and the gas is taken into account by adding a surface and a Coulomb term in the energy density of each cell (Avancini et al. 2012). The Coulomb and surface terms are given by:

$$\mathcal{F}_{\text{Coul}} = 2fe^2\pi\Phi R^2 (\rho_p^I - \rho_p^{II})^2, \quad (26)$$

$$\mathcal{F}_{\text{surf}} = 3f\sigma/R, \quad (27)$$

where $R = (3V^I/4\pi)^{1/3}$ is the radius of the nucleus, σ is the surface energy coefficient, and Φ is given by :

$$\Phi = \frac{1}{5} \left(2 + f - 3f^{1/3} \right). \quad (28)$$

For this work, we have used the functional form for the surface energy coefficient σ proposed in Ref. Lattimer & Swesty (1991) which was validated on extended Thomas-Fermi calculations, and only depends on the proton fraction of the nucleus $y_p^I = \rho_p^I/\rho^I$:

$$\sigma = \sigma_0 \frac{2^{p+1} + b_s}{y_p^{I-p} + b_s + (1 - y_p^I)^{-p}} h_t, \quad (29)$$

with

$$h_t = (1 - (T/T_c)^2)^2, \text{ if } T < T_c$$

$$h_t = 0, \text{ if } T \geq T_c,$$

$$T_c = 87.76 \left(\frac{K_0}{375} \right)^{1/2} \left(\frac{0.155}{\rho_0} \right)^{1/3} y_p^I (1 - y_p^I). \quad (30)$$

In this expression, σ_0 , b_s and p are free parameters that must be optimized for each nuclear model. To do so, we consider the prediction of the CLD model for the mass of a nucleus of mass number A and proton number Z in the vacuum:

$$\begin{aligned} M(A, Z) &= m_p Z + m_n (A - Z) \\ &+ \frac{A}{\rho_0(y_p)} \epsilon(\rho_0(y_p), \delta, T = 0) \\ &+ 4\pi R^2 \sigma + \frac{3Z^2}{5R}, \end{aligned} \quad (31)$$

where $y_p = Z/A$, $\delta = 1 - 2y_p$, the nuclear radius is $R = (4\pi\rho_0(y_p)/3)^{-1/3} A^{1/3}$, and the bulk density $\rho_0(y_p)$ is given by the equilibrium density of nuclear matter at proton fraction y_p , defined by $\partial\epsilon/\partial\rho|_{y_p, \rho_0(y_p), T=0} = 0$. For each model, the associated surface parameters σ_0 , b_s and p are determined by a χ^2 -fit of Eq. (31) to the experimental Atomic Mass Evaluation (AME) 2016 (Audi et al. 2017).

Finally, since we are considering finite temperature matter, a translational free energy term should also be considered, which accounts for the droplet center-of-mass motion at temperatures beyond the crystallization temperature. If we consider the thermal motion as for an ideal gas, the translational term reads (Haensel et al. 2007)

$$\begin{aligned} \mathcal{F}_{\text{trans}} &= \frac{F_{\text{trans}}}{V_W} = \frac{T}{V_W} \left[\ln \left(\frac{\lambda^3}{V_W A_{\text{heavy}}^{3/2}} \right) - 1 \right] \\ &= \frac{fT}{V^I} \left[\ln \left(\frac{f\lambda^3}{V^{I5/2} \rho^I{}^{3/2}} \right) - 1 \right], \end{aligned} \quad (32)$$

where the mass number of the heavy cluster is given by Eq. (23), and the nucleon thermal wavelength is given by $\lambda = \left(\frac{2\pi\hbar^2}{MT} \right)^{1/2}$. As discussed by many authors (Lattimer & Swesty 1991; Sedrakian 1996; Magierski & Bulgac 2004; Martin & Urban 2016; Dinh Thi et al. 2023b), the ideal gas approximation is not very realistic in the dense medium of the inner crust. Following Ref. Dinh Thi et al. (2023b), we therefore consider an effective mass number of the heavy cluster, A^* , where the gas density is removed to account for the fact that the unbound nucleons do not participate to the translational motion of the ion:

$$A^* = A_{\text{heavy}}(1 - \rho^{II}/\rho^I) = V^I(\rho^I - \rho^{II}). \quad (33)$$

Moreover, the finite size of the nucleus implies that the free volume available for the ion motion is reduced with respect to the whole volume of the cell (Lattimer et al. 1985). The volume fraction f (defined after Eq. (25)) should be replaced by $f^* = V^I/V_W^*$ with $V_W^* = 4/3\pi(R_W - R)^3$, where R_W is the radius of the Wigner-Seitz cell. This volume is related with the volume of the cluster by $V_W^* = V^I/f(1 - f^{1/3})^3$. If we substitute these expressions in Eq. (32), the translational free energy density becomes:

$$\begin{aligned} \mathcal{F}_{\text{trans}}^* &= \frac{F_{\text{trans}}^*}{V_W} = \frac{fT}{V^I} \left[\ln \left(\frac{\lambda^3}{V_W^* A^{*3/2}} \right) - 1 \right] \\ &= \frac{fT}{V^I} \left[\ln \left(\frac{f\lambda^3}{V^{I5/2} (\rho^I - \rho^{II})^{3/2} (1 - f^{1/3})^3} \right) - 1 \right] \end{aligned} \quad (34)$$

Note that in the applications shown in this paper, the proton gas is always negligible, and the results would not be changed by subtracting only the unbound neutrons in Eqs. (33)-(34).

By minimizing the sum $\mathcal{F}_{\text{surf}} + \mathcal{F}_{\text{Coul}} + \mathcal{F}_{\text{trans}}$ with respect to the size R of the droplet, one gets:

$$\mathcal{F}_{\text{surf}} = 2\mathcal{F}_{\text{Coul}} - 3\mathcal{F}_{\text{trans}} - \frac{15fT}{2V^I}. \quad (35)$$

This expression holds if we consider either the effective or ideal gas expression for the translational energy term.

With the addition of the surface, Coulomb and translational term, the total free energy density in the cell Eq. (25) is modified to:

$$\begin{aligned} \mathcal{F}_W &= f\mathcal{F}^I + (1-f)\mathcal{F}^{II} + \mathcal{F}_e \\ &+ \mathcal{F}_{\text{surf}} + \mathcal{F}_{\text{Coul}} + \mathcal{F}_{\text{trans}}. \end{aligned} \quad (36)$$

2.3. Inclusion of light clusters

In this work, besides considering a heavy cluster, we also add the different H and He isotopes to the system, namely deuterons $d \equiv {}^2\text{H}$, tritons $t \equiv {}^3\text{H}$, heliums $h \equiv {}^3\text{He}$, α -particles $\alpha \equiv {}^4\text{He}$ and ${}^6\text{He} \equiv {}^6\text{He}$, along the line of Ref. Pais et al. (2019). These light clusters are considered as structureless point-like, with an effective mass that depends on the density, and are added as new degrees of freedom to the system. In-medium effects are also taken into account in a two-fold way: via a parameter, x_s , that was fixed to experimental constraints, in the scalar cluster-meson coupling, and via a binding energy shift term, to take into account the Pauli principle, avoiding therefore double counting (Pais et al. 2019, 2020).

This amounts to adding to the Lagrangian density Eq. (1) the extra contribution of these new degrees of freedom:

$$\sum_{j=p,n} \mathcal{L}_j \rightarrow \sum_{j=p,n,d,t,h,\alpha,{}^6\text{He}} \mathcal{L}_j. \quad (37)$$

The Lagrangian density term for the fermionic clusters, t and h , has the same form as for the nucleons (see Eq. (2)) with the substitution $g_v \rightarrow A_j g_v$, $g_s \rightarrow x_s A_j g_s$, $M^* \rightarrow M_j^*$. Here, A_j is the mass number of the composite particle, its effective mass is given by

$$M_j^* = A_j M - x_s A_j g_s \phi_0 - (B_j^0 + \delta B_j), \quad (38)$$

where B_j^0 is the isotope binding energy in the vacuum, and δB_j and x_s are effective modifications of the binding energy and scalar meson coupling, accounting for the mass shift of the bound composite in the dense medium, see Ref. Pais et al. (2019) for details. For the scalar-isoscalar $J = 0$ particles (α and ${}^6\text{He}$) we have:

$$\mathcal{L}_j = \frac{1}{2} (iD_j^\mu \phi_j)^* (iD_{\mu j} \phi_j) - \frac{1}{2} \phi_j^* (M_j^*)^2 \phi_j, \quad (39)$$

with $iD_j^\mu = i\partial^\mu - A_j g_v \omega^\mu$, while the Lagrangian density of the vector-isoscalar $J = 1$ particle (deuteron) reads:

$$\begin{aligned} \mathcal{L}_j &= \frac{1}{4} (iD_j^\mu \phi_j^\nu - iD_j^\nu \phi_j^\mu)^* (iD_{j\mu} \phi_{j\nu} - iD_{j\nu} \phi_{j\mu}) \\ &- \frac{1}{2} \phi_j^{\mu*} (M_j^*)^2 \phi_{j\mu}. \end{aligned} \quad (40)$$

The number densities of the different light composites are given by Eq. (13) as for the nucleon densities, but the distributions depend on the quantum statistics:

$$f_{0j\pm} = \frac{1}{\eta + e^{(\epsilon_{0j} \mp \nu_j)/T}}, \quad (41)$$

with $\nu_j = \mu_j - A_j g_v V_0^{(0)}$, and $\eta = 1$ (-1) for fermions (bosons). Note that at the temperatures considered in the present study the α particles do not condensate.

The contribution of the light clusters is added to the bulk free energy \mathcal{F} and all other thermodynamic quantities defined in Eqs. (14), (15), (16), (17). The chemical equilibrium condition with the nucleons implies the definition of the chemical potentials for the composite particles ($j = d, t, h, \alpha, {}^6\text{He}$):

$$\mu_j = N_j \mu_n + Z_j \mu_p, \quad (42)$$

where $N_j(Z_j)$ is the neutron (proton) number of the composite.

The total baryon density and the condition of charge neutrality read

$$\rho = f\rho^I + (1-f)\rho^{II} + \sum_j A_j \rho_j, \quad (43)$$

$$\rho_p = f\rho_p^I + (1-f)\rho_p^{II} + \sum_j Z_j \rho_j, \quad (44)$$

$$= \rho_e = y_p \rho, \quad (45)$$

with $j = d, t, h, \alpha, {}^6\text{He}$, and y_p the global proton fraction. We note that Eq. (44) holds because $\rho_j^I = 0$.

Finally, we define the following quantities, as in Ref. Avancini et al. (2012): the mass fraction of the gas (unbound nucleons) is written as:

$$Y_{\text{free}} = (y_p^{II} + y_n^{II})(1-f)\rho^{II}/\rho, \quad (46)$$

with $y_{p(n)}^{I(II)} = \rho_{p(n)}^{I(II)}/\rho^{I(II)}$. The total mass fraction of the light composites is given by

$$Y_{\text{light}} = \sum_{j=d,t,h,\alpha,{}^6\text{He}} y_j^{II}(1-f)\rho^{II}/\rho, \quad (47)$$

and the mass fraction of the heavy ion is given by

$$Y_{\text{heavy}} = f\rho^I/\rho, \quad (48)$$

with $y_j^{I(II)}$ the mass fraction bound in each of the light clusters

$$y_j^{I(II)} = A_j \frac{\rho_j^{I(II)}}{\rho^{I(II)}}. \quad (49)$$

2.4. Equilibrium composition

The fractions of the different components of the Wigner-Seitz cell in equilibrium are determined from the minimization of the total free energy (Baym et al. 1971; Lattimer et al. 1985; Bao et al. 2014; Pais et al. 2015), which in our model includes the light clusters as well as the surface, Coulomb, and translational terms of the heavy cluster. This minimization is done with respect to four variables: the size of the nuclear droplet, R , its baryonic and proton density, ρ^I , ρ_p^I , and its volume fraction within the

cell, f . The equilibrium conditions become:

$$\mu_n^I = \mu_n^{II} + \frac{3T}{2V^I \rho^I} - \frac{\mathcal{F}_{\text{surf}}}{f} \beta_p, \quad (50)$$

$$\begin{aligned} \mu_p^I &= \mu_p^{II} - \frac{2\mathcal{F}_{\text{Coul}}}{f(1-f)(\rho_p^I - \rho_p^{II})} \\ &+ \frac{3T}{2V^I \rho^I} + \frac{\mathcal{F}_{\text{surf}}}{f} \beta_n, \end{aligned} \quad (51)$$

$$\begin{aligned} P^I &= P^{II} - \frac{2\mathcal{F}_{\text{Coul}}}{(\rho_p^I - \rho_p^{II})} \left(\frac{\rho_p^I}{f} + \frac{\rho_p^{II}}{(1-f)} \right) \\ &+ \mathcal{F}_{\text{Coul}} \left(\frac{3}{f} + \frac{1}{\Phi} \frac{\partial \Phi}{\partial f} \right) + \frac{\mathcal{F}_{\text{surf}}}{f} (\beta_n \rho_p^I - \beta_p \rho_n^I) \\ &- \frac{5T}{V^I} - \frac{2\mathcal{F}_{\text{trans}}}{f}, \end{aligned} \quad (52)$$

with

$$\begin{aligned} \beta_n &= \frac{\rho_n^I}{\rho^{I^2}} \left\{ p \frac{(1-y_p^I)^{-1-p} - y_p^{I^{-1-p}}}{y_p^{I^{-p}} + b_s + (1-y_p^I)^{-p}} + \frac{1}{h_t} \frac{dh_t}{dy_p^I} \right\}, \\ \beta_p &= \frac{\rho_p^I}{\rho^{I^2}} \left\{ p \frac{(1-y_p^I)^{-1-p} - y_p^{I^{-1-p}}}{y_p^{I^{-p}} + b_s + (1-y_p^I)^{-p}} - \frac{1}{h_t} \frac{dh_t}{dy_p^I} \right\}, \\ y_p^I &= \frac{\rho_p^I}{\rho^I}. \end{aligned} \quad (53)$$

If instead we consider the effective translational energy, we get

$$\mu_n^I = \mu_n^{II} + \frac{3T}{2V^I(\rho^I - \rho^{II})(1-f)} - \frac{\mathcal{F}_{\text{surf}}}{f} \beta_p, \quad (54)$$

$$\begin{aligned} \mu_p^I &= \mu_p^{II} - \frac{2\mathcal{F}_{\text{Coul}}}{f(1-f)(\rho_p^I - \rho_p^{II})} + \frac{3T}{2V^I(\rho^I - \rho^{II})} \\ &+ \frac{\mathcal{F}_{\text{surf}}}{f} \beta_n, \end{aligned} \quad (55)$$

$$\begin{aligned} P^I &= P^{II} - \frac{2\mathcal{F}_{\text{Coul}}}{(\rho_p^I - \rho_p^{II})} \left(\frac{\rho_p^I}{f} + \frac{\rho_p^{II}}{(1-f)} \right) \\ &+ \mathcal{F}_{\text{Coul}} \left(\frac{3}{f} + \frac{1}{\Phi} \frac{\partial \Phi}{\partial f} \right) + \frac{\mathcal{F}_{\text{surf}}}{f} (\beta_n \rho_p^I - \beta_p \rho_n^I) \\ &+ \frac{3fT}{2V^I(\rho^I - \rho^{II})} \left(\frac{\rho^I}{f} + \frac{\rho^{II}}{1-f} \right) \\ &- \frac{T}{V^I} \left(\frac{15}{2} - \frac{1}{1-f^{1/3}} \right) - \frac{2\mathcal{F}_{\text{trans}}^*}{f} \end{aligned} \quad (56)$$

We note that there are additional terms in both the chemical potentials and the mechanical equilibrium conditions compared to those that would be obtained in a simple thermodynamic phase equilibrium $\mu^I = \mu^{II}$, $P^I = P^{II}$. These terms result from the inclusion of the surface, Coulomb, and translational energy terms in the total energy minimization. The Coulomb repulsion and the translational energy induce additional positive terms, while the surface tension reduces the internal cluster pressure. Since we are considering a surface tension parameterization that depends on $y_p^I = \rho_p^I/\rho^I$, there is also an extra term that appears in the equilibrium conditions.

2.5. Impurity parameter

Let us now define the impurity factor, Q_{imp} . The number densities of the heavy ion and of the light composites are given by:

$$\rho_{\text{heavy}} = \rho \frac{Y_{\text{heavy}}}{A_{\text{heavy}}} = \frac{1}{V_W} \quad (57)$$

$$\rho_{\text{light}} = \sum_{j=\text{d,t,h},\alpha,{}^6\text{He}} \rho_j \quad (58)$$

with Y_{heavy} given by Eq. (48), and the number of nucleon in the heavy cluster being given by Eq. (23). With these definitions, we can now write the number fraction of the heavy cluster and of the light clusters:

$$X_{\text{heavy}} = \frac{\rho_{\text{heavy}}}{\rho_{\text{heavy}} + \rho_{\text{light}}}, \quad (59)$$

$$X_j = \frac{\rho_j}{\rho_{\text{heavy}} + \rho_{\text{light}}}. \quad (60)$$

The average and square average atomic number of clusters in a single cell, whatever their size, can then be written as

$$\langle Z \rangle = Z_{\text{heavy}} X_{\text{heavy}} + \sum_{j=\text{d,t,h},\alpha,{}^6\text{He}} Z_j X_j, \quad (61)$$

$$\langle Z^2 \rangle = Z_{\text{heavy}}^2 X_{\text{heavy}} + \sum_{j=\text{d,t,h},\alpha,{}^6\text{He}} Z_j^2 X_j, \quad (62)$$

which allows us to write $Q_{\text{imp}} = \langle Z^2 \rangle - \langle Z \rangle^2$, with Z_{heavy} given by Eq. (24).

Table 1. Optimized surface parameters, namely σ_0 , b_s , and p , for the models considered in this work, fitted to the AME2016 mass table (Audi et al. 2017).

	σ_0	b_s	p
	(MeV/fm ²)		
FSU	1.17734	21.18512	3.0
FSU2R	1.15978	25.63181	3.0
NL3 $\omega\rho$	1.15068	25.20164	3.0
NLset21	1.08889	37.73938	3.0
DD-ME2	1.09358	5.47648	2.42
DD2	1.03886	21.67598	3
TW	1.14452	19.79133	3

3. Results and Discussions

The calculations in this paper are performed using four non-linear models, FSU, FSU2R, NL3 $\omega\rho$, NLset21, and three density dependent models, TW, DD2, and DDME2, to illustrate the model dependence of the results. These models fulfill several constraints, as discussed in Sect. 2. As mentioned in Sect. 2.3, apart from the heavy cluster, we also include five light clusters, namely ${}^2\text{H}$, ${}^3\text{H}$, ${}^3\text{He}$, ${}^4\text{He}$ and ${}^6\text{He}$. We perform the calculations at β -equilibrium, which is expected to be achieved in late cooling stages of proto-NS (Camelio et al. 2017), and for temperatures close to the expected crystallization temperature of the NS crust. The optimal surface parameters obtained from the fit to the experimental mass table AME2016 for these models are displayed in Table 1. Moreover, the symmetric nuclear matter

Table 2. Symmetric nuclear matter saturation properties for all models considered in this work: saturation density ρ_0 (fm^{-3}), binding energy per nucleon E/A , incompressibility K_0 , skewness Q_0 , kurtosis Z_0 , symmetry energy coefficient $J_{\text{sym},0}$, slope $L_{\text{sym},0}$, curvature $K_{\text{sym},0}$, skewness $Q_{\text{sym},0}$, and kurtosis $Z_{\text{sym},0}$ of the symmetry energy (all in MeV).

model	ρ_0	E/A	K_0	Q_0	Z_0	$J_{\text{sym},0}$	$L_{\text{sym},0}$	$K_{\text{sym},0}$	$Q_{\text{sym},0}$	$Z_{\text{sym},0}$
FSU	0.148	-16.32	228	-521	2815	32.5	60	-51	426	-6332
FSU2R	0.1505	-16.26	238	135	4982	30.7	47	56	190	-10917
NL3 $\omega\rho$	0.148	-16.24	270	198	9304	31.6	55	-8.07	1396	-13602
NLset21	0.156	-16.12	216	-339	6785	29	42	55	1146	14120
DDME2	0.152	-16.14	251	479	4448	32.	51	-87	776	-7047
DD2	0.149065	-16.02	243	168	5233	31.7	55	-93	598	-5152
TW	0.153	-16.24	240	-539	3749	32.5	55	-124.7	538	-3307

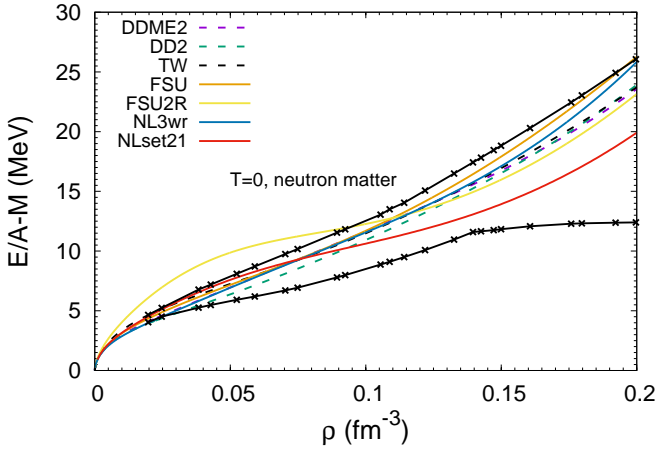


Fig. 1. Energy per baryon of pure neutron matter as a function of the total baryon density at $T = 0$ MeV for all the models considered in this work. The lines with stars indicate the overlapping region of several chiral-EFT calculations, taken from Ref. Huth et al. (2022).

parameters calculated at saturation density are listed in Table 2. The models differ mainly in the density dependence of the symmetry energy.

To evaluate the reliability of the different models, we start by checking if the RMF models, non-linear and density dependent, are consistent with the latest ab-initio pure neutron matter calculations from chiral-EFT theory. To this aim, we plot in Fig. 1, the energy per neutron as a function of density. We observe that only the FSU2R model fails this constraint, although the parametrization was constrained by the pure neutron-matter pressure from the ab-initio calculation obtained in Ref. Hagen et al. (2015).

In Fig. 2, we plot in the top panel the surface tension at β -equilibrium for the representative temperature $T = 1$ MeV just slightly above the expected temperature of crystallization of the innermost part of the inner crust (Carreau et al. 2020; Dinh Thi, H. et al. 2021), for the two classes of RMF models, non-linear (solid) and density-dependent (dashed). For comparison, the surface tension for a fixed proton fraction $y_p = 0.3$, a value close to the neutron dripline, is also shown. The difference between the two results represents the effect on the surface energy of the density dependence of the isospin content of the heavy

cluster in β equilibrium. In the middle panel, for the same temperature and models, we show the proton fraction in the dense phase against the baryonic density obtained for β -equilibrium matter (thick) and matter with fixed proton fraction (thin). The global proton fraction at β -equilibrium is plotted as a function of the density in the bottom panel. As one can see from Eq. (29), the surface tension depends only on the proton fraction of the cluster y_p^I . The strong decrease of the surface energy with density thus reflects the increasing neutron richness of the equilibrium nucleus, which in turn is due to the decreasing global proton fraction as a function of density (see bottom panel). This general feature, as well as the disappearance of the surface tension at the crust–core transition, is common to all models. This behavior is in contrast to the case of a constant proton fraction. There, the proton fraction of the nucleus decreases very slowly (see middle panel), from ~ 0.4 in the very low density limit to the global value, 0.3, close to the dissolution of the clusters. This behavior is in turn reflected in the surface tension (see top panel).

In Fig. 3, we plot the absolute value of the ratio between the translational free energy term and the sum of the Coulomb and surface terms. Again, the specificity of the NS crust governed by β -equilibrium (thick lines) can be appreciated by the comparison with the fixed proton fraction case, also shown in the figure (thin lines). In the β -equilibrium case, from the very low density limit up to $\sim 0.03 \text{ fm}^{-3}$, the translational free energy term (with or without considering an effective mass number of the cluster) is much smaller than the sum of the Coulomb and surface terms. If the proton fraction of the droplet does not vary much with density, as is the case for $y_p = 0.3$, the translational term in the inner crust becomes completely negligible, particularly for $\rho \gtrsim 0.01 \text{ fm}^{-3}$, at least at the relatively low temperatures corresponding to crustal crystallization. However, the effect is reversed in the innermost part of the inner crust when the β equilibrium is considered, which is due to the strong decrease of the surface tension in the very neutron rich β equilibrated matter observed in Fig. 2. This is in line with the results shown in Ref. Dinh Thi et al. (2023b), see their Fig. 6. As discussed at length in that work, in the global minimization of the cell free energy, the Coulomb plus surface term tend to favor the low-energy configurations as it is the case at $T = 0$, corresponding to highly bound heavy clusters. Conversely, the translational term tends to favor high-entropy config-

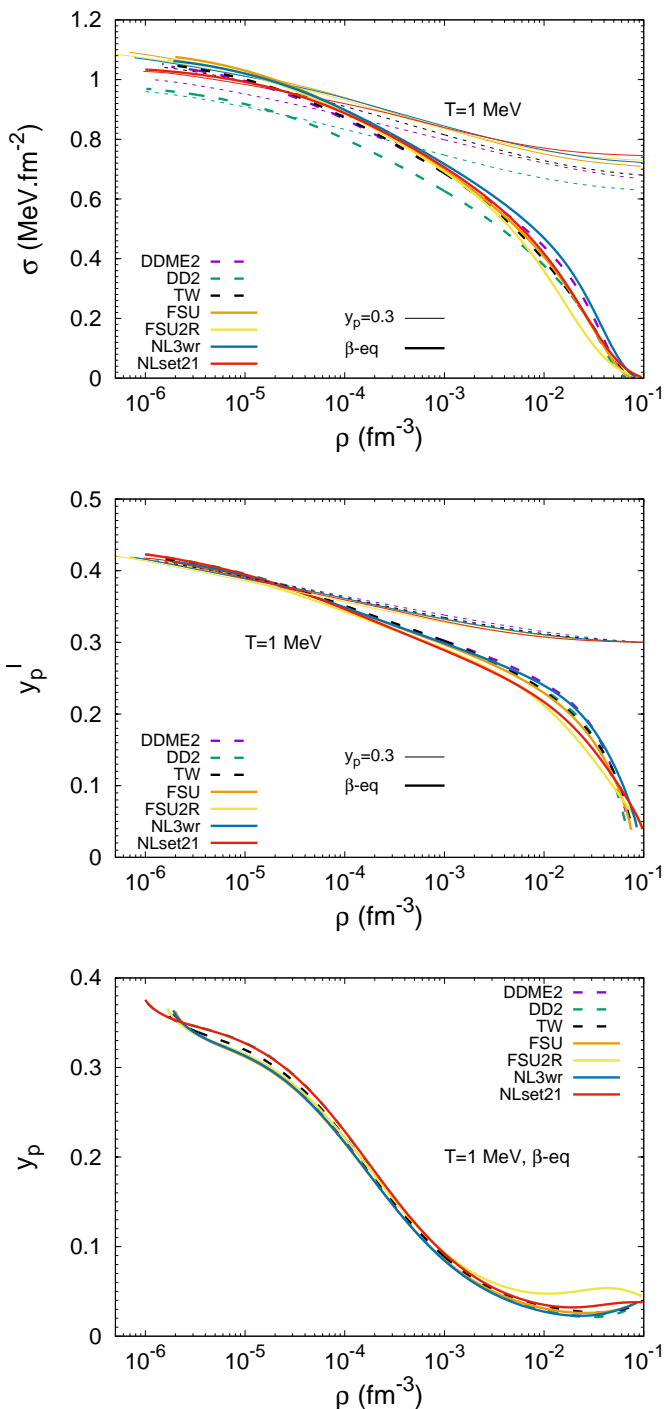


Fig. 2. Cluster surface tension σ (top panel), proton fraction in the dense phase y_p^I (middle panel) and global proton fraction y_p (bottom panel) in the inner crust at $T = 1$ MeV as a function of the total baryon density ρ obtained for β -equilibrium matter (thick lines) and matter with fixed proton fraction $y_p = 0.3$ (thin lines in top and middle panels) for all the models considered in this work. The results are obtained without the translational term, and the surface parameters are obtained from the fit to the mass table AME2016 (Audi et al. 2017).

urations as in a classical gas, corresponding to small mass numbers for the droplet. The increase of the ratio between the two terms at high density means that the heavy clus-

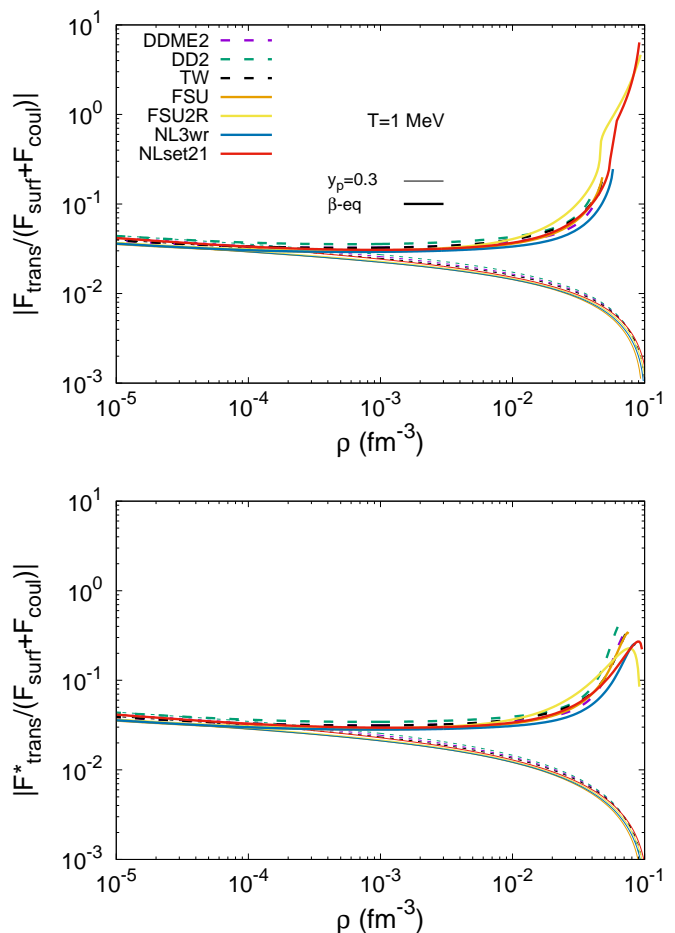


Fig. 3. Absolute value of the translational free energy divided by the sum of the Coulomb and surface energies as a function of the total baryon density ρ obtained in a CLD calculation with five light clusters at $T = 1$ MeV in β -equilibrium matter (thick lines) and matter with fixed proton fraction $y_p = 0.3$ (thin lines) for all the models considered in this work. The top (bottom) panels are obtained with the translational term of ideal-gas, F_{trans} (with the corrections on the finite-size and in-medium effects, F_{trans}^*).

ters are going to melt in the dense medium in a much more effective way when this term is accounted for.

This simplified picture occurs if we neglect the effect of the dripped neutrons on the translational motion of the droplet. With the inclusion of the effective mass number for the cluster, the translational degree of freedom is reduced in the dense medium which lowers this ratio and moderates the effect. Still, the effect of including the translational degrees of freedom in the variational equations is very important, as it can be seen from Fig. 4.

Indeed, in this figure, we show how the number of protons (left) and nucleons (right) in the heavy cluster evolves with the density, fixing the temperature at $T = 1$ MeV. We only consider the FSU and DD2 models, but the qualitative results are the same for all the models used in this work. We consider the three different cases: without (violet) and with the translational free energy, the latter considering both its ideal-gas version (green) and including the effective mass number of the cluster (black). The composition of matter in the NS crust (lower panel, β equilibrium) is very different from the case of dilute nuclear matter at

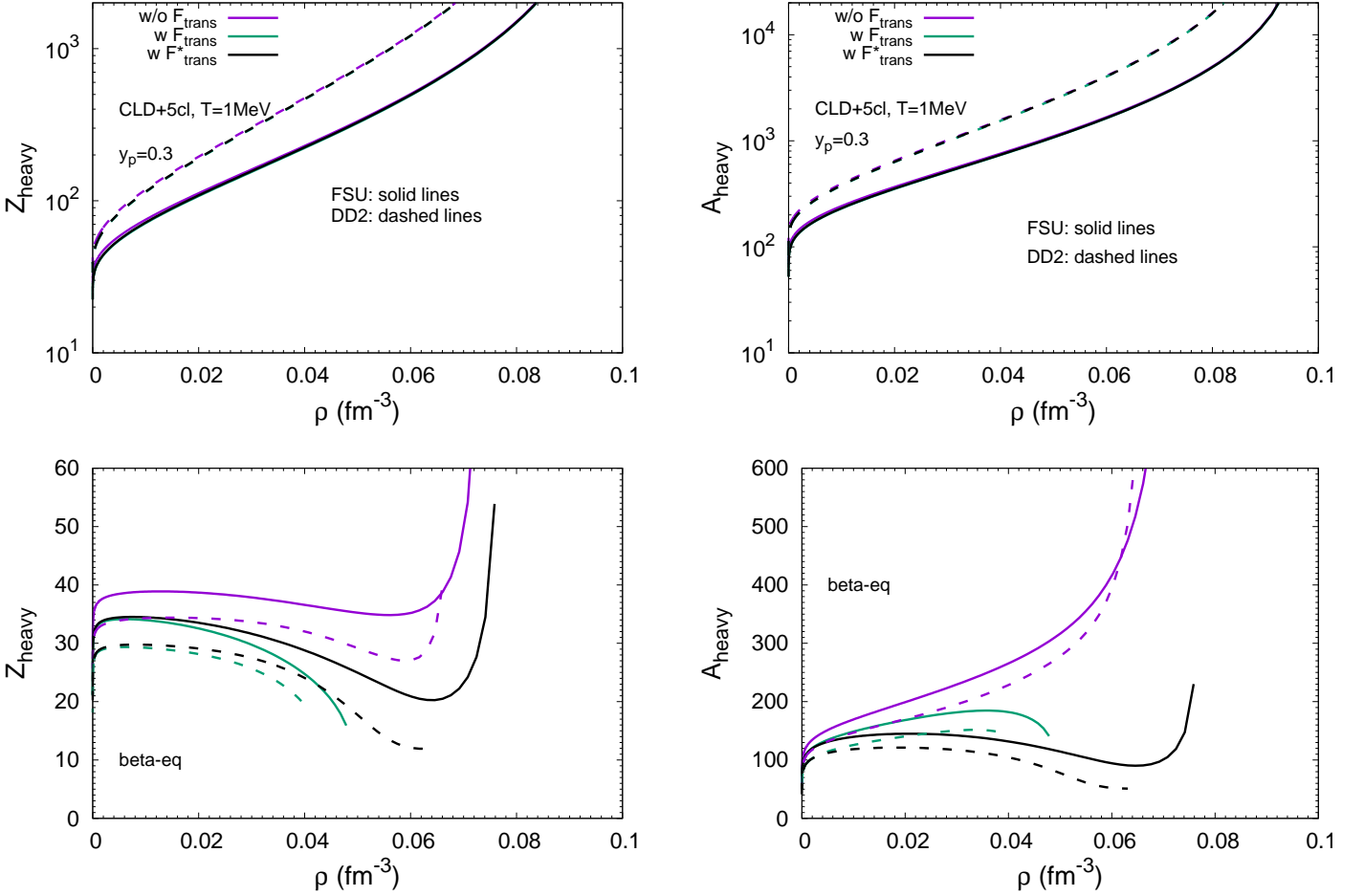


Fig. 4. Number of protons (left) and nucleons (right) in the heavy cluster as a function of the total baryon density ρ in a CLD calculation with 5 light clusters for the FSU (solid lines) and DD2 (dashed lines) interactions with a fixed proton fraction of $y_p = 0.3$ (top panels) and β -equilibrium (bottom panels), at $T = 1$ MeV. The different colors represent the results obtained without the translational free energy (violet lines), with the ideal-gas translational term F_{trans} (green lines) and the corrected translational term F_{trans}^* (black lines).

constant proton fraction (upper panel). Looking at the top panels, the two models and the three different calculations behave similarly: the number of protons and of nucleons increase until the homogeneous matter is achieved. For the β -equilibrium calculation (bottom panels), the behavior is different: for both models, neglecting the translational term (violet lines) the composition of the liquid crust is very close to what is expected for the catalyzed ground-state composition, with an atomic number slowly varying according to the crustal depth, in the range $Z_{\text{heavy}} \approx 30 - 40$ (left panel), and a faster increase for the nucleon number, in the range $A_{\text{heavy}} \approx 100 - 400$ (right panel), and a sharp increase at the crust-core transition where matter becomes homogeneous. The difference between including or not the effective mass number in the translational term, i.e. the difference between considering F_{trans}^* , Eq. (34), instead of F_{trans} , Eq. (32), is to make the decrease of the droplet proton and nucleon numbers smoother. With the effective translational energy term (black lines), and for densities above $\sim 0.06 \text{ fm}^{-3}$, the behavior of FSU is similar to the case without F_{trans} : the number of protons and of nucleons increases at the crust-core transition where the clusters dissolve. The DD2 model follows a different trend and does not show a steep increase

at the crust-core transition. No heavy droplets survive at $T = 1$ MeV above a density of $\rho \approx 0.04 - 0.05 \text{ fm}^{-3}$ using F_{trans} , as we can see from the bottom left panel (green lines). This is because the effective number of nucleons has a strong correlation with the density of the gas ρ^{II} (recalling that $A^* = A_{\text{heavy}}(1 - \rho^{II}/\rho^I) = V^I(\rho^I - \rho^{II})$). In β equilibrium, this quantity is quite high and close to the density of the cluster, when the baryonic density approaches the dissolution density of the clusters, making the cluster size to further decrease, $V^I = fV_W^*(1 - f^{(1/3)})^{-3}$. This is in line with Ref. Dinh Thi et al. (2023b), see their Figs. 7, 9 and 11.

In Fig. 5, we show the mass fractions as a function of the density for the light (top panel), and heavy (middle panel) clusters, together with the unbound nucleons (bottom panel). We only consider the most realistic prescription for the translational term with the effective mass number of the cluster, Eq. (34), and both non-linear (solid lines) and density-dependent (dashed lines) models at the representative temperature of $T = 1$ MeV. The abundance of light clusters is systematically more important in the case of non-linear models, but it is globally small for all models, particularly in the inner crust region. This can be under-

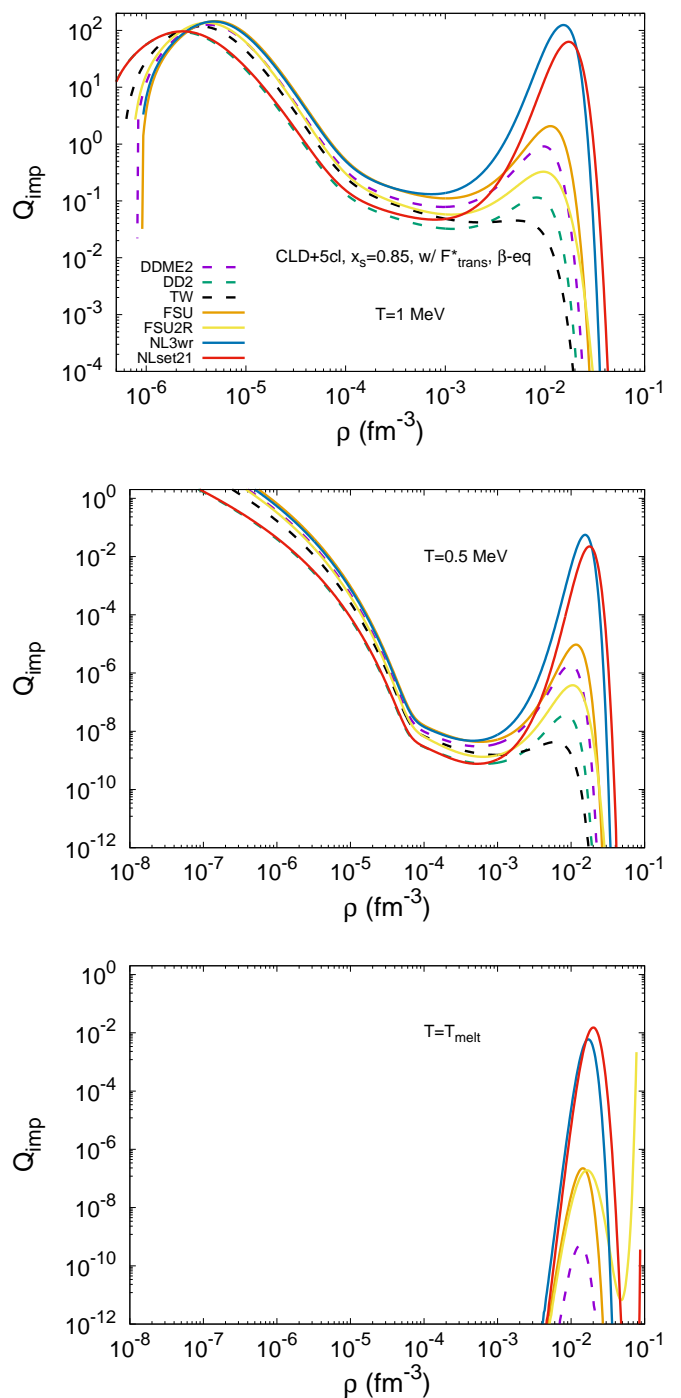
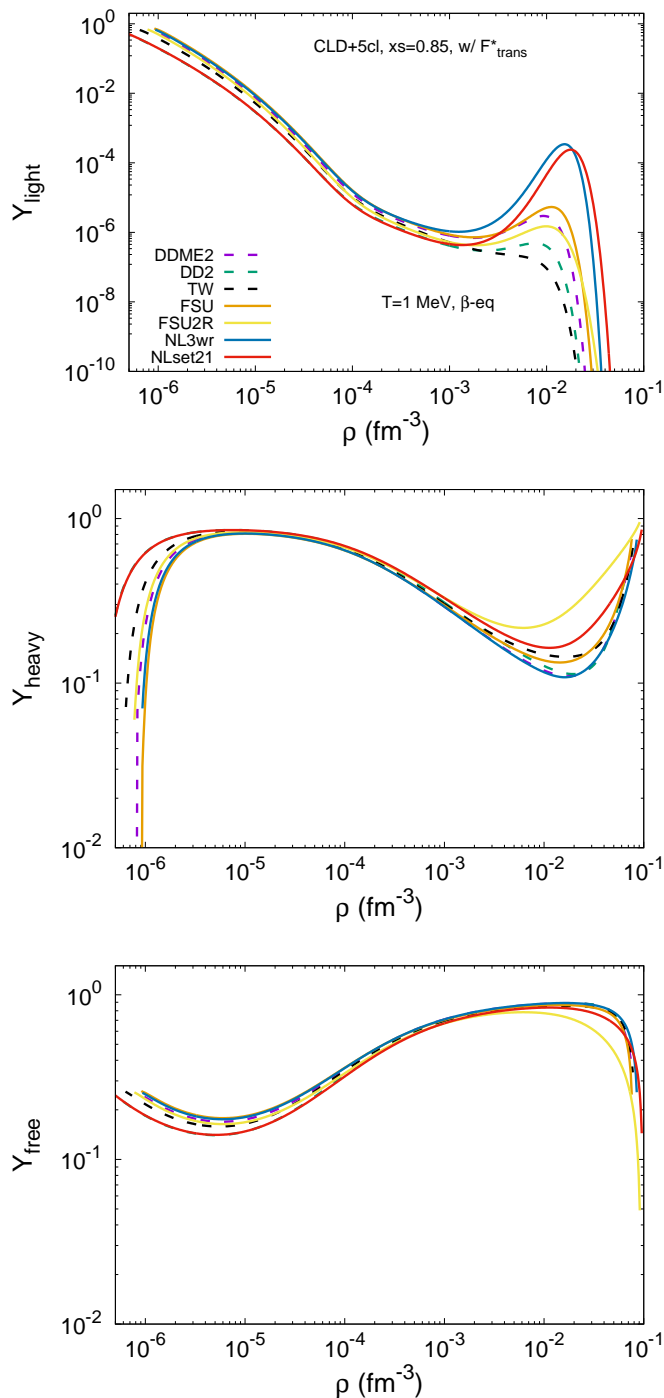


Fig. 5. Mass fractions of the light clusters (top panel), heavy cluster (middle panel), and of the unbound nucleons (bottom panel), as a function of the total baryon density ρ in the inner crust at $T = 1$ MeV for all the models considered in this work. The results are obtained employing the corrected translational term F_{trans}^* .

Fig. 6. Impurity parameter Q_{imp} as a function of the total baryon density ρ in a CLD calculation with 5 light clusters for all the models considered in this work in β -equilibrium, and at $T = 1$ MeV (top panel), $T = 0.5$ (middle panel), and at the crystallization temperature $T = T_{\text{melt}}$ (bottom panel). Results are obtained employing the corrected translational term F_{trans}^* .

stood from the fact that the mass fraction of the heavy cluster dominates in most of the crust, implying that the volume fraction of dilute matter is too small to accommodate an important contribution of light composites together with unbound neutrons. Compared to Ref. Dinh Thi et al. (2023b), where a full multi-component plasma calculation suggested a dominance of He and Li isotopes in the inner-

most part of the inner crust, we observe that in this study these clusters were extremely neutron-rich, with mass numbers of the order of $A_{\text{heavy}} \approx 20$.

We turn now to the discussion of the impurity parameter. In Fig. 6, we show the impurity parameter calculated at $T = 1$ MeV (top panel), 0.5 MeV (middle panel), and at the crystallization temperature $T = T_{\text{melt}}$ (bottom panel),

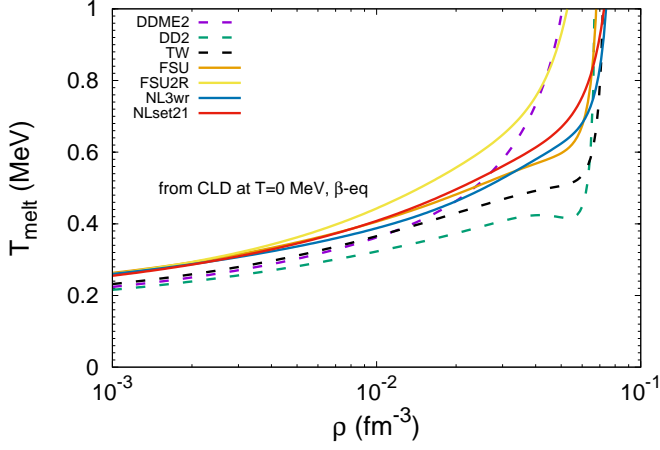


Fig. 7. Crystallization temperature, T_{melt} , as a function of the total baryon density ρ , with Z_{heavy} and R_W obtained in a CLD calculation at $T = 0$ and β -equilibrium for all the models considered in this work.

estimated as (Haensel et al. 2007)

$$T_{\text{melt}} = \frac{Z_{\text{heavy}}^2 e^2}{175 \times R_W}, \quad (63)$$

with Z_{heavy} and R_W calculated from a CLD calculation at $T = 0$ and in β equilibrium. The crystallization temperature is plotted as a function of the density in Fig. 7. We notice that, as the density increases, the DD models present a lower impurity parameter as compared to the NL models. This is due to the fact that for the DD models the light-cluster mass fractions is lower, as can be seen in Fig. 5. Also, when we decrease the temperature to 0.5 MeV, the Q_{imp} values are much lower, especially for the DD models. The same happens when we calculate this parameter at the crystallization temperature: indeed, for DD2 and TW, this quantity is zero, since already at $T = 0.5$ MeV and $\rho \gtrsim 0.01 \text{ fm}^{-3}$, $Q_{\text{imp}} \lesssim 10^{-8}$ (see middle panel of Fig. 6), and $T_{\text{melt}} \gtrsim 0.5$ MeV for $\rho > 0.04 \text{ fm}^{-3}$ (see Fig. 7). Similarly, for DDME2, Q_{imp} is also very low (notice the scale). On the other hand, for NL3 $\omega\rho$ and NLset21, we have a peak of about $Q_{\text{imp}} \sim 10^{-2}$ at $\rho \sim 10^{-2} \text{ fm}^{-3}$. We also notice that as the temperature decreases, the peak reached for each model decreases in magnitude but it happens at about the same density, as we can see from Fig. 8. This is very different from the results found in Ref. Dinh Thi et al. (2023a) (see their Fig. 15), where light H and He isotopes were not considered, but a full multi-component plasma calculation was performed accounting for fluctuations of the heavy cluster. Indeed, in Ref. Dinh Thi et al. (2023a), the change in temperature does not seem to particularly affect the amplitude of the maximum of Q_{imp} , but it shifts the density at which the peak occurs.

4. Conclusions

In this paper, we have calculated the abundance of light clusters (namely, the different isotopes of H and He) in thermodynamic conditions corresponding to the crystallization of the NS crust, using different RMF models and treating the light composites as independent structure-less quasi-particles. Such light clusters are expected to be formed in

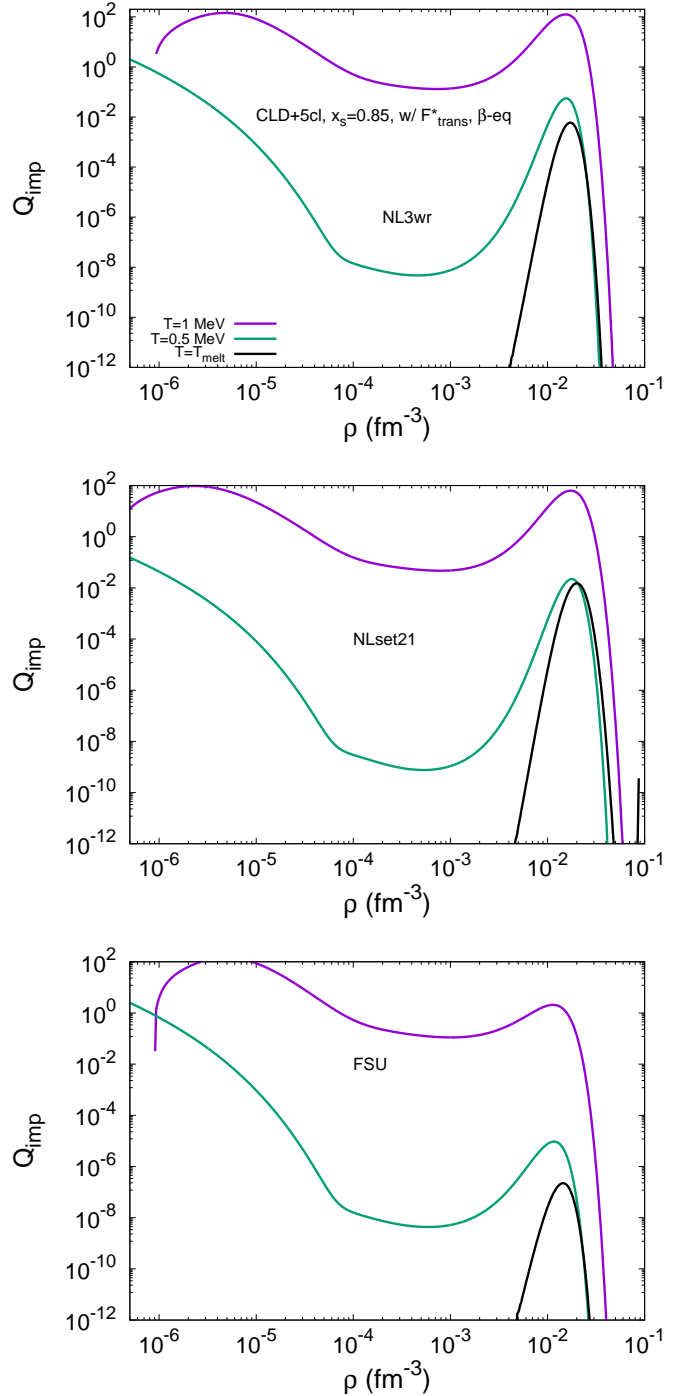


Fig. 8. Impurity parameter Q_{imp} as a function of the total baryon density ρ in a CLD calculation with 5 light clusters at β equilibrium for $T = 1$ MeV (dark blue lines), $T = 0.5$ MeV (green lines) and $T = T_{\text{melt}}$ (black lines), for NL3 $\omega\rho$ (top panel), NLset21 (middle panel), and FSU (bottom panel). The results consider the corrected translational term F_{trans}^* .

the dilute nucleon gas that characterizes the inner crust of the star while still in the liquid phase, and could therefore persist in the catalyzed crust due to the suppression of pycnonuclear reactions (Chamel et al. 2020) below the crystallization temperature. The purpose of this study was to quantify the possible contribution due to such composite

particles to the impurity factor that determines the resistivity of the NS crust.

In all models, the contribution to the impurity factor that can be attributed to the presence of light cluster is negligible. This means that the nucleon fluid made of dripped neutrons and protons in the inner crust can be safely treated as an homogeneous fluid as in the mean-field approximation. As a consequence, if high Q_{imp} values exist in the inner crust as it is suggested by different astrophysical observations (Pons et al. 2013; Newton 2013; Deibel et al. 2017; Hambaryan et al. 2017; Tan et al. 2018), its microscopic origin is likely to lie in the presence of either a deformed pasta mantle with defects (Schneider et al. 2014; Horowitz et al. 2015; Caplan et al. 2021; Newton et al. 2022), or of the fluctuations of the charge of the dominant (heavy) ion in each cell (Carreau et al. 2020; Fantina et al. 2020; Dinh Thi et al. 2023b), fluctuations that were not considered in this work.

ACKNOWLEDGMENTS

This work was partially supported by national funds from FCT (Fundação para a Ciência e a Tecnologia, I.P., Portugal) under projects UIDB/04564/2020 and UIDP/04564/2020, with DOI identifiers 10.54499/UIDB/04564/2020 and 10.54499/UIDP/04564/2020, respectively, and the project 2022.06460.PTDC with the associated DOI identifier 10.54499/2022.06460.PTDC. H.P. acknowledges the grant 2022.03966.CEECIND (FCT, Portugal) with DOI identifier 10.54499/2022.03966.CEECIND/CP1714/CT0004. F.G., A.F. and H.D.T. acknowledge the support by the IN2P3 Master Project NewMAC and MAC, the ANR project ‘Gravitational waves from hot neutron stars and properties of ultra-dense matter’ (GW-HNS, ANR-22-CE31-0001-01), the CNRS International Research Project (IRP) ‘Origine des éléments lourds dans l’univers: Astres Compacts et Nucléosynthèse (ACNu)’.

References

- Arcones, A., Martínez-Pinedo, G., O’Connor, E., et al. 2008, *Phys. Rev. C*, 78, 015806
- Audi, G., Kondev, F. G., Wang, M., Huang, W. J., & Naimi, S. 2017, *Chin. Phys. C*, 41, 030001
- Avancini, S. S., Barros, Jr, C. C., Brito, L., et al. 2012, *Phys. Rev. C*, 85, 035806
- Bao, S. S., Hu, J. N., Zhang, Z. W., & Shen, H. 2014, *Phys. Rev. C*, 90, 045802
- Bauswein, A., Goriely, S., & Janka, H. T. 2013, *Astrophys. J.*, 773, 78
- Baym, G., Bethe, H. A., & Pethick, C. 1971, *Nucl. Phys. A*, 175, 225
- Bougault, R. et al. 2020, *J. Phys. G*, 47, 025103
- Camelio, G., Lovato, A., Gualtieri, L., et al. 2017, *Phys. Rev. D*, 96, 043015
- Caplan, M. E., Forsman, C. R., & Schneider, A. S. 2021, *Phys. Rev. C*, 103, 055810
- Carreau, T., Fantina, A. F., & Gulminelli, F. 2020, *Astron. Astrophys.*, 640, A77, [Erratum: *Astron. Astrophys.* 645, C1 (2021)]
- Chamel, N., Fantina, A. F., Zdunik, J.-L., & Haensel, P. 2020, *Phys. Rev. C*, 102, 015804
- Custódio, T., Falcão, A., Pais, H., et al. 2020, *Eur. Phys. J. A*, 56, 295
- Custódio, T., Rebillard-Soulié, A., Bougault, R., et al. 2024 [arXiv:2407.02307]
- Deibel, A., Cumming, A., Brown, E. F., & Reddy, S. 2017, *Astrophys. J.*, 839, 95
- Dinh Thi, H., Fantina, A. F., & Gulminelli, F. 2023a, *Astron. Astrophys.*, 677, A174
- Dinh Thi, H., Fantina, A. F., & Gulminelli, F. 2023b, *Astron. Astrophys.*, 672, A160
- Dinh Thi, H., Fantina, A. F., & Gulminelli, F. 2021, *Eur. Phys. J. A*, 57, 296
- Fantina, A. F., De Ridder, S., Chamel, N., & Gulminelli, F. 2020, *Astron. Astrophys.*, 633, A149
- Ferreira, M. & Providencia, C. 2012, *Phys. Rev. C*, 85, 055811
- Fischer, T., Hempel, M., Sagert, I., Suwa, Y., & Schaffner-Bielich, J. 2014, *Eur. Phys. J. A*, 50, 46
- Fischer, T., Typel, S., Röpke, G., Bastian, N.-U. F., & Martínez-Pinedo, G. 2020, *Phys. Rev. C*, 102, 055807
- Furnstahl, R. J., Serot, B. D., & Tang, H.-B. 1996, *Nucl. Phys. A*, 598, 539
- Furnstahl, R. J., Serot, B. D., & Tang, H.-B. 1997, *Nucl. Phys. A*, 615, 441, [Erratum: *Nucl. Phys. A* 640, 505–505 (1998)]
- Furusawa, S., Nagakura, H., Sumiyoshi, K., & Yamada, S. 2013, *Astrophys. J.*, 774, 78
- Furusawa, S., Sumiyoshi, K., Yamada, S., & Suzuki, H. 2017, *Nucl. Phys. A*, 957, 188
- Goriely, S., Chamel, N., Janka, H. T., & Pearson, J. M. 2011, *Astron. Astrophys.*, 531, A78
- Grill, F., Pais, H., Providência, C., Vidaña, I., & Avancini, S. S. 2014, *Phys. Rev. C*, 90, 045803
- Haensel, P., Potekhin, A. Y., & Yakovlev, D. G. 2007, *Neutron stars 1: Equation of state and structure*, Vol. 326 (New York, USA: Springer)
- Hagen, G. et al. 2015, *Nature Phys.*, 12, 186
- Hambaryan, V., Suleimanov, V., Haberl, F., et al. 2017, *Astron. Astrophys.*, 601, A108
- Horowitz, C. J., Berry, D. K., Briggs, C. M., et al. 2015, *Phys. Rev. Lett.*, 114, 031102
- Horowitz, C. J. & Piekarewicz, J. 2001, *Phys. Rev. Lett.*, 86, 5647
- Huth, S. et al. 2022, *Nature*, 606, 276
- Lalazisiss, G. A., Nikšić, T., Vretenar, D., & Ring, P. 2005, *Phys. Rev. C*, 71, 024312
- Lattimer, J. M., Pethick, C. J., Ravenhall, D. G., & Lamb, D. Q. 1985, *Nucl. Phys. A*, 432, 646
- Lattimer, J. M. & Swesty, F. D. 1991, *Nucl. Phys. A*, 535, 331
- Magierski, P. & Bulgac, A. 2004, *Nucl. Phys. A*, 738, 143
- Malik, T., Pais, H., & Providência, C. 2024, *Astron. Astrophys.*, 689, A242
- Malik, T. & Providência, C. 2022, *Phys. Rev. D*, 106, 063024
- Martin, N. & Urban, M. 2016, *Phys. Rev. C*, 94, 065801
- Nedora, V., Bernuzzi, S., Radice, D., et al. 2021, *Astrophys. J.*, 906, 98
- Negreiros, R., Tolos, L., Centelles, M., Ramos, A., & Dexheimer, V. 2018, *Astrophys. J.*, 863, 104
- Newton, W. G. 2013, *Nature Phys.*, 9, 396
- Newton, W. G., Kaltenborn, M. A., Cantu, S., et al. 2022, *Phys. Rev. C*, 105, 025806
- Pais, H., Chiacchiera, S., & Providência, C. 2015, *Phys. Rev. C*, 91, 055801
- Pais, H., Gulminelli, F., Providência, C., & Röpke, G. 2018, *Phys. Rev. C*, 97, 045805
- Pais, H., Gulminelli, F., Providência, C., & Röpke, G. 2019, *Phys. Rev. C*, 99, 055806
- Pais, H. & Providência, C. 2016, *Phys. Rev. C*, 94, 015808
- Pais, H. et al. 2020, *Phys. Rev. Lett.*, 125, 012701
- Pons, J. A., Viganò, D., & Rea, N. 2013, *Nature Phys.*, 9, 431
- Potekhin, A. Y. & Chabrier, G. 2021, *Astron. Astrophys.*, 645, A102
- Psaltis, A., Jacobi, M., Montes, F., et al. 2024, *Astrophys. J.*, 966, 11
- Qin, L., Hagel, K., Wada, R., et al. 2012, *Phys. Rev. Lett.*, 108, 172701
- Radice, D., Perego, A., Hotokezaka, K., et al. 2018, *Astrophys. J.*, 869, 130
- Ren, Z., Elhatisari, S., Lähde, T. A., Lee, D., & Meißner, U.-G. 2024, *Phys. Lett. B*, 850, 138463
- Röpke, G. 2015, *Phys. Rev. C*, 92, 054001
- Röpke, G. 2020, *Phys. Rev. C*, 101, 064310
- Rosswog, S. 2015, *Int. J. Mod. Phys. D*, 24, 1530012
- Schneider, A. S., Berry, D. K., Briggs, C. M., Caplan, M. E., & Horowitz, C. J. 2014, *Phys. Rev. C*, 90, 055805
- Sedrakian, A. D. 1996, *Ap&SS*, 236, 267
- Shchechilin, N. N., Chamel, N., & Pearson, J. M. 2023, *Phys. Rev. C*, 108, 025805
- Shchechilin, N. N., Chamel, N., Pearson, J. M., Chugunov, A. I., & Potekhin, A. Y. 2024, *Phys. Rev. C*, 109, 055802
- Sumiyoshi, K. & Röpke, G. 2008, *Phys. Rev. C*, 77, 055804
- Tan, C. M. et al. 2018, *Astrophys. J.*, 866, 54
- Todd-Rutel, B. G. & Piekarewicz, J. 2005, *Phys. Rev. Lett.*, 95, 122501
- Typel, S., Röpke, G., Klahn, T., Blaschke, D., & Wolter, H. H. 2010, *Phys. Rev. C*, 81, 015803
- Typel, S. & Wolter, H. H. 1999, *Nucl. Phys. A*, 656, 331
- Viganò, D., Rea, N., Pons, J. A., et al. 2013, *Mon. Not. Roy. Astron. Soc.*, 434, 123